

Application of Bootstrap to θ -term

Yu AIKAWA^{a*}, Takeshi MORITA^{a,b†} and Kota YOSHIMURA^{c‡}

*a. Department of Physics, Shizuoka University
836 Ohya, Suruga-ku, Shizuoka 422-8529, Japan*

*b. Graduate School of Science and Technology, Shizuoka University
836 Ohya, Suruga-ku, Shizuoka 422-8529, Japan*

*c. Department of Physics, University of Notre Dame
Notre Dame, Indiana, 46556, USA*

Abstract

Recently, novel numerical computation on quantum mechanics by using a bootstrap method was proposed by Han, Hartnoll, and Kruthoff. We consider whether this method works in systems with a θ -term, where the standard Monte-Carlo computation may fail due to the sign problem. As a starting point, we study quantum mechanics of a charged particle on a circle in which a constant gauge potential is a counterpart of a θ -term. We find that it is hard to determine physical quantities as functions of θ such as $E(\theta)$, except at $\theta = 0$ and π . On the other hand, the correlations among observables for energy eigenstates are correctly reproduced for any θ . Our results suggest that the bootstrap method may work not perfectly but sufficiently well, even if a θ -term exists in the system.

*E-mail address: aikawa.yu.17(at)shizuoka.ac.jp

†E-mail address: morita.takeshi(at)shizuoka.ac.jp

‡E-mail address: kyoshimu(at)nd.edu

1 Introduction

Numerical analysis plays essential role in modern physics. Without the help of numerical analysis, quantitative evaluation is very difficult in many cases. Particularly, Monte-Carlo computation (MC) is quite powerful and is widely employed in various studies. However, MC may not be available when there are sign problems. Hence, various alternative numerical approaches such as complex Langevin method [1, 2, 3, 4, 5, 6], tensor renormalization method [7] and Lefschetz thimble method [8, 9] are being studied actively. (See a review article [10] for recent progress on lattice QCD.)

Recently, as a novel numerical tool, the bootstrap method was proposed [11, 12] in zero-dimensional matrix models. This method was developed to quantum mechanics [13], and several studies confirmed its validity [14, 15, 16]. Particularly, this method works in gauge theories at large- N limit [11, 12, 13, 14, 16]. (Indeed, finite N is harder in this method.) Since taking large- N limit is difficult in MC, the bootstrap method may provide a new window of numerical study of large- N gauge theories.

Then, it is natural to ask whether the bootstrap method is applicable to systems with sign problems. In this letter, we study a θ -term, which is pure imaginary in Euclidean action and causes a sign problem. Since the application of the bootstrap method to higher dimensional quantum field theories has not been established, as a starting point, we study quantum mechanics of a charged particle on a circle.

$$\begin{aligned} S(\theta) &= \int dt \left(\frac{1}{2} \dot{x}^2 - V(x) \right) - \frac{\theta}{2\pi} \int dt \dot{x}, \\ V(x) &= a(1 - \cos(x)). \end{aligned} \tag{1.1}$$

Here, we impose a periodicity $x = x + 2\pi$ and a is a non-negative coupling constant. θ is a real constant parameter and can be regarded as a background constant gauge potential, which causes the Aharonov-Bohm effect. The last term becomes a pure imaginary in the Euclidean action, and it is a counterpart of the θ -term in QCD. Although this model is very simple, several similarities between this model and the θ -term in QCD are known [17], and this model may provide us an intuition whether the bootstrap method potentially works in QCD or not.

We apply the numerical bootstrap method to this model and find that it is difficult to determine physical quantities as functions of θ such as $E(\theta)$. On the other hand, the correlations among observables for energy eigenstates are correctly obtained for any θ . For

example, we can describe the expectation value of a position operator $\langle E|e^{ix}|E\rangle$ as a function of energy eigenvalues. In addition, $\theta = 0$ and π are special, and physical quantities can be determined there. These results suggest that the bootstrap method works not perfectly but sufficiently well, even if a θ -term exists in systems.

The organization of this article is as follows. In section 2, we review the model (1.1) and derive the spectra and several quantities. In section 3, we employ the numerical bootstrap method and compare the obtained results with the ones derived in Sec. 2. Section 4 contains conclusions and discussions.

Note: After we submitted our manuscript to arxiv, related works were done independently in Refs. [18, 19]. Particularly, a derivation of the θ dependence of observables was proposed in Ref. [19].

2 Analytic Study of the Model

In this section, we study the model (1.1) analytically, and we will compare the results in this section with the bootstrap analysis in the next section. We will call the results in this section as “analytic results” in order to distinguish the results obtained through the bootstrap method.

From (1.1), we obtain the Hamiltonian

$$H(\theta) := \frac{1}{2} \left(p + \frac{\theta}{2\pi} \right)^2 - a(\cos(x) - 1), \quad (2.1)$$

and we investigate the Schrödinger equation

$$E\psi(x) = H(\theta)\psi(x), \quad (2.2)$$

where $\psi(x)$ is an energy eigenfunction and E is its energy eigenvalue.

Importantly, this system has a gauge symmetry. Indeed, by multiplying $e^{i\frac{\lambda}{2\pi}x}$ from the left in (2.2), we obtain

$$Ee^{i\frac{\lambda}{2\pi}x}\psi(x) = e^{i\frac{\lambda}{2\pi}x}H(\theta)e^{-i\frac{\lambda}{2\pi}x}e^{i\frac{\lambda}{2\pi}x}\psi(x) = H(\theta - \lambda)e^{i\frac{\lambda}{2\pi}x}\psi(x), \quad (2.3)$$

where λ is a real constant parameter and we have used $e^{i\frac{\lambda}{2\pi}x}pe^{-i\frac{\lambda}{2\pi}x} = p - \lambda/2\pi$. Thus, θ and the wave function are transformed as

$$\theta \rightarrow \theta - \lambda, \quad \psi(x) \rightarrow e^{i\frac{\lambda}{2\pi}x}\psi(x). \quad (2.4)$$

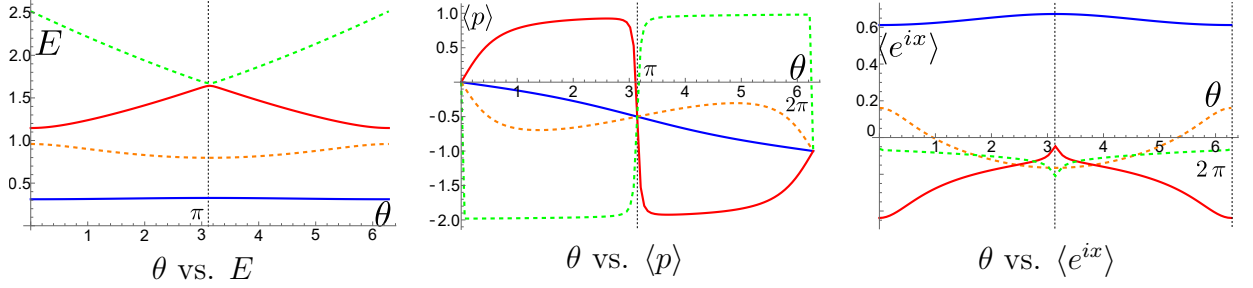


Figure 1: θ dependence of E , $\langle p \rangle$ and $\langle e^{ix} \rangle$. We numerically solve the Schrödinger equation (2.1) with the boundary condition $\psi(x+2\pi) = \psi(x)$. The curves are for the first four energy eigenstates: The blue curves, the orange dashed ones, the red ones and the green dashed ones are the first, the second, the third and the fourth state, respectively. We take $a = 1/2$ in these plots.

Particularly, this transformation changes the periodicity of the wave function by λ . For example, if the original wave function is periodic, the periodicity becomes

$$\psi(x+2\pi) = \psi(x) \rightarrow \tilde{\psi}(x) := e^{i\frac{\lambda}{2\pi}x}\psi(x), \quad \tilde{\psi}(x+2\pi) = e^{i\lambda}\tilde{\psi}(x). \quad (2.5)$$

Correspondingly, the momentum $\langle p \rangle$ is transformed as

$$\langle p \rangle \rightarrow \langle p \rangle + \frac{1}{2\pi}\lambda. \quad (2.6)$$

Thus, the momentum $\langle p \rangle$ is not a gauge invariant observable. On the other hand, the velocity

$$\langle \dot{x} \rangle := \langle p \rangle + \frac{\theta}{2\pi}, \quad (2.7)$$

is gauge invariant.

Because of this gauge redundancy, we need to fix a gauge in order to solve the Schrödinger equation. In the following analysis, we fix the periodicity of the wave function periodic: $\psi(x+2\pi) = \psi(x)$. However, we can still apply a gauge transformation (2.4) with $\lambda = 2\pi$, which retains this periodicity, and $(\theta, \langle p \rangle)$ is identical to $(\theta - 2\pi, \langle p \rangle + 1)$. Thus, the physical domain of θ can be taken as $0 \leq \theta < 2\pi$.

Under this gauge fixing condition, we solve the Schrödinger equation (2.2) and evaluate the energy spectrum, $\langle p \rangle$ and $\langle e^{ix} \rangle$ for the energy eigenstates¹. The results at $a = 1/2$ are summarized in Fig. 1. Here, we plot these quantities for the first four energy eigenstates with respect to θ .

¹The Schrödinger equation (2.2) may be solved in terms of Mathieu functions, but we use Mathematica package NDEigensystem.

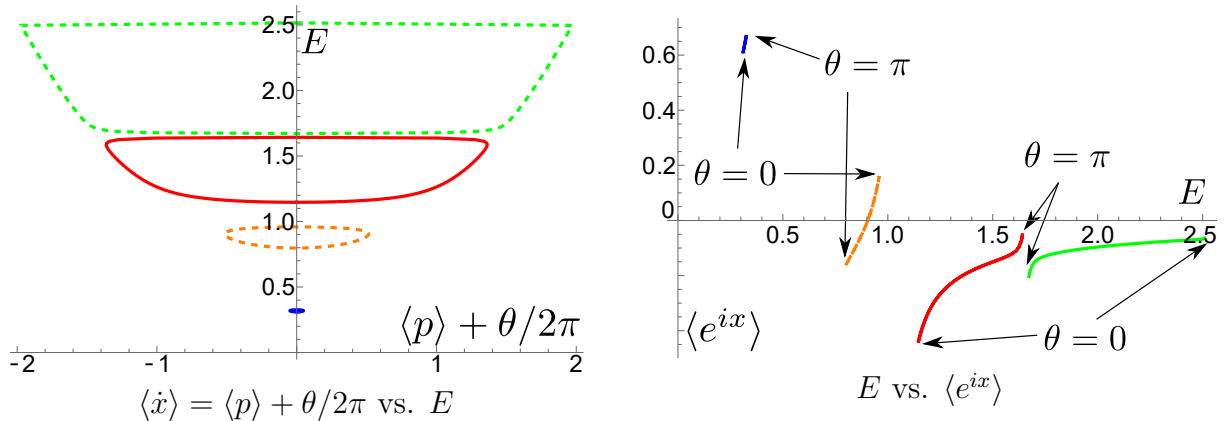


Figure 2: Correlations among the gauge invariant quantities: E , $\langle \dot{x} \rangle$ and $\langle e^{ix} \rangle$. The curves are for the first four energy eigenstates considered in Fig. 1. The line styles correspond to those in Fig. 1.

However, θ and $\langle p \rangle$ are not gauge invariant, and the correlations between the gauge invariant quantities may be more important. Hence, we plot $\langle \dot{x} \rangle$ vs. E and E vs. $\langle e^{ix} \rangle$ in Fig. 2. We will later see that the bootstrap method reproduces these correlations correctly.

In Appendix A, the analysis at $a = 0$ is shown. There, the calculations are very simple, and they may provide intuitions about the properties of the solutions at $a > 0$ plotted in Fig. 1 and 2.

3 Bootstrap Analysis

We analyze (2.1) via the bootstrap method and will compare the results with the analytic ones obtained in the previous section.

In order to use the bootstrap method, we consider the following operators²,

$$O_{mn} := e^{imx} p^n, \quad m = 0, \pm 1, \pm 2, \dots, \quad n = 0, 1, 2, \dots. \quad (3.1)$$

Then, we define

$$\tilde{O} = \sum_{m=0}^{K_x} \sum_{n=0}^{K_p} c_{mn} O_{mn} = c_{00} + c_{10} e^{ix} + c_{01} p + \dots, \quad (3.2)$$

where $\{c_{nm}\}$ are constants, and K_p and K_x are non-negative integers. Since $\langle \alpha | O^\dagger O | \alpha \rangle \geq 0$

²Note that we consider the operators e^{imx} rather than x^m . This is because the operators x^m are not well defined in quantum mechanics on S^1 . For example, it does not satisfy $\langle [H, x] \rangle = 0$ even if the state is an energy eigenstate. We can easily confirm it in the $a = 0$ case by using (A.1).

is satisfied for any state $|\alpha\rangle$ in this system for arbitrary well-defined operators O ,

$$\langle\alpha|\tilde{O}^\dagger\tilde{O}|\alpha\rangle \geq 0 \quad (3.3)$$

is satisfied for any constants $\{c_{nm}\}$. Hence, the following $(K_p+1)(K_x+1) \times (K_p+1)(K_x+1)$ matrix \mathcal{M} has to be positive-semidefinite [13],

$$\mathcal{M} := \begin{pmatrix} 1 & \langle\alpha|e^{ix}|\alpha\rangle & \langle\alpha|p|\alpha\rangle & \cdots \\ \langle\alpha|e^{-ix}|\alpha\rangle & 1 & \langle\alpha|e^{-ix}p|\alpha\rangle & \cdots \\ \langle\alpha|p|\alpha\rangle & \langle\alpha|pe^{ix}|\alpha\rangle & \langle\alpha|p^2|\alpha\rangle & \cdots \\ \vdots & \vdots & \vdots & \ddots \end{pmatrix} \succeq 0, \quad (3.4)$$

This strongly constrains the possible values of the observables $\langle\alpha|O_{mn}|\alpha\rangle$. We call \mathcal{M} as a bootstrap matrix. Note that, as K_x and K_p increase, the constraint becomes typically stronger.

From now on, we focus on energy eigenstates and take $|\alpha\rangle$ as an energy eigenstate $|E\rangle$. Then, $\langle E|O_{mn}|E\rangle$ has to satisfy the following two conditions [13]:

$$\langle E|[H, O_{mn}]|E\rangle = 0, \quad (3.5)$$

$$\langle E|HO_{mn}|E\rangle = E\langle E|O_{mn}|E\rangle. \quad (3.6)$$

Here E is the energy eigenvalue of the eigenstate $|E\rangle$. (In the following, we omit $|E\rangle$.) By substituting (3.1) to these two equations, we obtain

$$m^2O_{mn} + 2mO_{mn+1} + \frac{m\theta}{\pi}O_{mn} + a \left[\sum_{k=0}^{n-1} {}_n C_k (O_{m+1k} + (-1)^{n-k}O_{m-1k}) \right] = 0, \quad (3.7)$$

and

$$\begin{aligned} & \frac{1}{2} \left[m^2O_{mn} + 2mO_{mn+1} + O_{mn+2} + \frac{m\theta}{\pi}O_{mn} + \frac{\theta}{\pi}O_{mn+1} - a(O_{m+1n} + O_{m-1n}) \right] \\ & = \left(E - \frac{\theta^2}{8\pi^2} - a \right) O_{mn}. \end{aligned} \quad (3.8)$$

The summation in (3.7) appears when the operators in the equation are ordered into the forms (3.1) through the commutator relation $[p, e^{imx}] = me^{imx}$. By solving these equations³, we can describe all the observables $\langle O_{mn} \rangle$ by the three variables: $\langle p \rangle$, $\langle e^{ix} \rangle$ and E . For example, from (3.7) with $(m, n) = (1, 0)$, we obtain

$$\langle e^{ix}p \rangle = - \left(\frac{1}{2} + \frac{\theta}{2\pi} \right) \langle e^{ix} \rangle. \quad (3.9)$$

³We use Mathematica to solve (3.7) and (3.8).

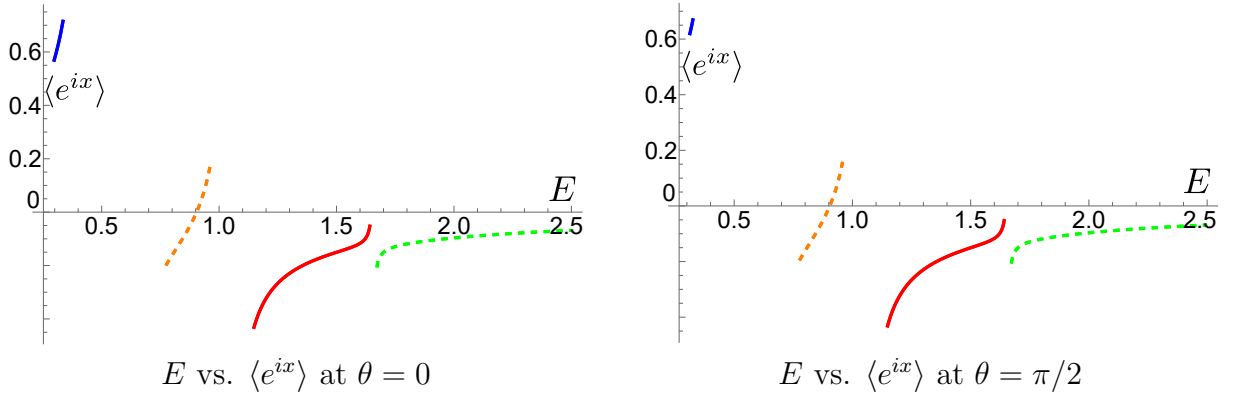


Figure 3: E vs. $\langle e^{ix} \rangle$ through the bootstrap analysis. We take $a = 1/2$ and investigate $\theta = 0$ and $\pi/2$. We fix E and find the minimum (maximum) value of $\langle e^{ix} \rangle$ numerically, although the convergence is very good and we cannot distinguish the minimum and maximum in these plots. The curves are for the first four energy eigenstates considered in Fig. 1 and Fig. 2. The line styles are the same as explained in Fig. 1. We find that the curves do not depend on θ almost and they are identical to the analytic results in Fig. 2.

By substituting them into the bootstrap matrix \mathcal{M} , we obtain,

$$\mathcal{M} = \begin{pmatrix} 1 & \langle e^{ix} \rangle & \langle p \rangle & \cdots \\ \langle e^{ix} \rangle & 1 & \left(\frac{1}{2} - \frac{\theta}{2\pi}\right) \langle e^{ix} \rangle & \cdots \\ \langle p \rangle & \left(\frac{1}{2} - \frac{\theta}{2\pi}\right) \langle e^{ix} \rangle & -2a + 2E - \frac{\theta^2}{4\pi^2} + 2a \langle e^{ix} \rangle - \frac{\theta}{\pi} \langle p \rangle & \cdots \\ \vdots & \vdots & \vdots & \ddots \end{pmatrix}. \quad (3.10)$$

The idea of the bootstrap method is excluding the values of the variables $\langle p \rangle$, $\langle e^{ix} \rangle$ and E that do not satisfy the constraint $\mathcal{M} \succeq 0$. Particularly, if the size of the bootstrap matrix \mathcal{M} is sufficiently large, the allowed values might be very limited, and they might be almost identical to the values of the variables evaluated by energy eigenstates.

More concretely, we fix θ and E , and numerically find the possible minimum and maximum values of $\langle p \rangle$ (or $\langle e^{ix} \rangle$) that satisfy the condition $\mathcal{M} \succeq 0$ ⁴. By repeating these computations by changing E , we obtain the results summarized in Fig. 3 and 4 for $\theta = 0$ and $\pi/2$ at $a = 1/2$.

Firstly, we mention the convergence of our numerical results. They converge sufficiently first. Fig. 3 and 4 are for $K_p = 3$ and $K_x = 4$, but, even if the size of the bootstrap matrix is increased, there is no change in the appearance of these figures.

Now, we discuss the details of our numerical results. First, we consider the plot for E

⁴The bootstrap matrix \mathcal{M} linearly depends on $\langle p \rangle$ and $\langle e^{ix} \rangle$ while non-linearly depends on E . Thus, when we fix E , the problem finding the minimum (or maximum) of $\langle p \rangle$ (or $\langle e^{ix} \rangle$) that satisfies $\mathcal{M} \succeq 0$ reduces to so called ‘‘Semidefinite Programming Problem’’, and the numerical costs drastically decrease. We use Mathematica package SemidefiniteOptimization in our numerical analysis.

vs. $\langle e^{ix} \rangle$ depicted in Fig. 3. Surprisingly, the results do not depend on θ almost. $\theta = 0$ and $\theta = \pi/2$ provide nearly same results. Besides, the obtained curves are almost same to the analytic result shown in Fig. 2 (right). However, there is a crucial difference. The curve in Fig. 2 is the result for $0 \leq \theta < 2\pi$. Thus, if we fix θ to a single value, it corresponds to a single point on the curve. (More precisely, the plot in Fig. 2 is for the four states, and four points appear at this θ .) On the other hand, the curves in Fig. 3 are derived both at the single values of θ .

This difference between the analytic result and the bootstrap method can be explained as follows. In the former analysis, we have taken the gauge $\psi(x + 2\pi) = \psi(x)$. In the bootstrap analysis, however, we have not fixed the gauge. Thus, even if θ in the Hamiltonian (2.1) is taken to be zero, if the periodicity of the state is $\theta/2\pi$, the situation is equivalent to $H(\theta)$ with the periodic state through the gauge transformation (2.4):

$$H(0)\psi = E\psi, \quad \psi(x + 2\pi) = e^{i\theta/2\pi}\psi(x) \quad \iff \quad H(\theta)\psi = E\psi, \quad \psi(x + 2\pi) = \psi(x). \quad (3.11)$$

Hence, the bootstrap method derives the results for all possible values of θ in the Hamiltonian, even though we have taken $\theta = 0$ and $\pi/2$ in Fig. 3.

If we wish to obtain the result for a fixed θ corresponding to Fig. 2, we need to specify the periodicity of the states and fix the gauge. However, we could not find a good way. For example, we can read off the periodicity of the state by using the operator $e^{2\pi ip}$. Indeed, if the wave function has a periodicity $\psi(x + 2\pi) = e^{i\eta}\psi(x)$, the corresponding state satisfies $\langle e^{2\pi ip} \rangle = e^{i\eta}$. Thus, in order to fix the periodicity of the state, for example, $\psi(x + 2\pi) = \psi(x)$, we should impose the additional constraint $\langle e^{2\pi ip} \rangle = 1$ in the bootstrap analysis. However, the operator $e^{2\pi ip}$ commutes with all O_{mn} in (3.1), and the condition $\langle e^{2\pi ip} \rangle = 1$ does not restrict the values of O_{mn} . Hence, this method might not work⁵.

The difficulty of fixing the periodicity of the states causes a problem that we cannot determine the θ -dependence of the observables such as $E(\theta)$ and $\langle e^{ix} \rangle(\theta)$, since we always obtain the result for all θ . This is a disadvantage of our bootstrap analysis.

Now, we move to discuss the details of the plot for $\langle \dot{x} \rangle$ vs. E in Fig. 4. Again, the results are almost independent of θ ⁶, and the shapes of these curves agree with the analytic result in

⁵After the authors submitted the first manuscript of this work to arxiv, a related study [19] appeared independently. There, a possible way for determining $\langle e^{2\pi ip} \rangle$ was proposed, and it may overcome the issue of the gauge fixing.

⁶Note that if we plot E vs. $\langle p \rangle$ rather than $\langle \dot{x} \rangle$ via the bootstrap method, the results are almost same to Fig. 4 but the center of the curves $\langle \dot{x} \rangle = 0$ moves to $\langle p \rangle = -\theta/2\pi$. Thus, the results slightly depend on θ . But $\langle p \rangle$ is not a physical observable and the gauge invariant quantity $\langle \dot{x} \rangle$ does not depend on θ .

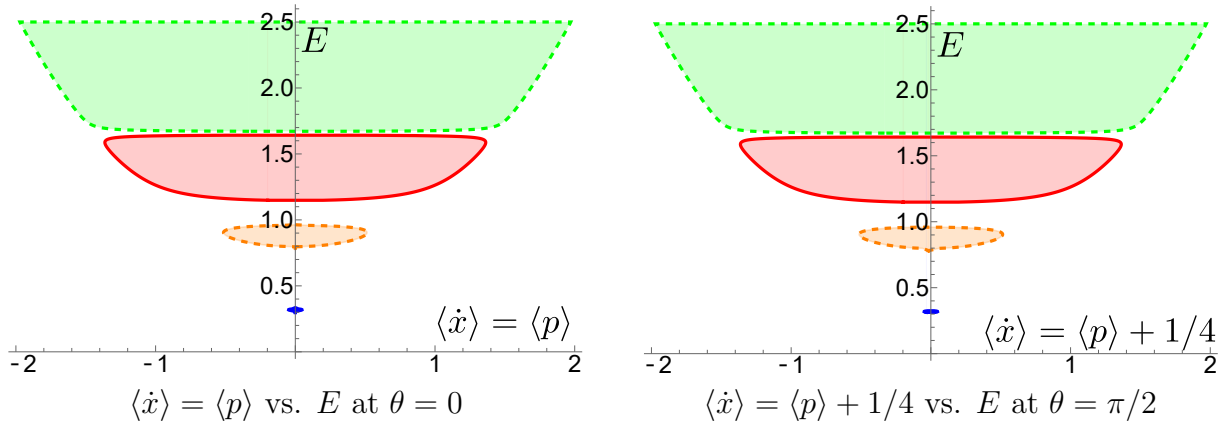


Figure 4: $\langle \dot{x} \rangle = \langle p \rangle + \theta/2\pi$ vs. E for the first four eigenstates through the bootstrap analysis. We take $a = 1/2$ and investigate $\theta = 0$ (left panel) and $\pi/2$ (right panel). We fix E and find the minimum (maximum) value of $\langle p \rangle$ numerically. The shaded regions are allowed region that satisfy $\mathcal{M} \geq 0$. These regions do not depend on the values of θ , and the boundaries of the regions are almost identical to the curves derived in the analytic calculation shown in Fig. 2 (left).

Fig. 2 (left) for all θ . This is similar to the E vs. $\langle e^{ix} \rangle$ case. However, there is one difference. The inside regions of the curves satisfy the condition $\mathcal{M} \geq 0$ and they are not excluded in the bootstrap analysis, while no solution appears there in the analytic result.

This subtle issue can be understood as follows. Suppose that we fix E and ask what is the possible value of $\langle \dot{x} \rangle$. From Fig. 2 (left), we see that there are two possible values, say $\pm \dot{x}(E)$. Then, the general solution at given E may be described as superposition of these two solutions. If so, the possible values of the expectation value $\langle \dot{x} \rangle$ may be in the following range,

$$-\dot{x}(E) \leq \langle \dot{x} \rangle \leq \dot{x}(E). \quad (3.12)$$

This corresponds to the bootstrap results shown in Fig. 4. However, this is not the end of the story. Since the point on the curves in Fig. 2 is for the solution at a single θ , the values of θ at $\dot{x}(E)$ and $-\dot{x}(E)$ are different. Thus, we cannot superpose the solutions for $\dot{x}(E)$ and $-\dot{x}(E)$, and the regions inside the curves in Fig. 4 should be excluded.

On the other hand, we have not fixed the periodicity of the states in the bootstrap analysis, and superposition of the $\pm \dot{x}(E)$ solutions have not been excluded. This is consistent with the result in Fig. 4. (Recall that different θ corresponds to the different periodicity through the gauge transformation (2.4).) As we have argued, it is hard to fix the periodicity in the bootstrap method, and we cannot exclude the inside region. However, it may not be

a serious issue, since we can easily read off the correct correlations between $\langle \dot{x} \rangle$ and E : they appear at the boundaries of the regions in Fig. 4.

In this way, we have obtained the correlations among $\langle e^{ix} \rangle$, $\langle \dot{x} \rangle$ and E . As we have mentioned, other operators $\langle O_{mn} \rangle$ are described by these three quantities, and we can easily obtain correlations among all the observables.

Finally, we briefly mention the relation to the Bloch's theorem [17]. The Bloch's theorem states that the system ($-\infty < x < \infty$) with a periodic potential would have a band structure. Since we have not fixed the periodicity of the states, we may regard that our system is in $-\infty < x < \infty$ rather than S^1 ⁷. Then, the energy curves in Fig. 3 and 4 naturally correspond to the band structure.

3.1 $\theta = 0$ and π

So far, we have seen that the bootstrap method can derive the correlations among the observables, but it cannot derive the θ dependence of them. Here, we argue that actually $\theta = 0$ and π are special, and we can read off the values of the observables there.

The Hamiltonian (2.1) is invariant under the parity symmetry: $(x, p, \theta) \rightarrow (-x, -p, -\theta)$. Thus, the eigenstates can be taken parity even or odd, and the expectation value of p at a given θ satisfies

$$p(-\theta) = -p(\theta), \quad (3.13)$$

where we have omitted the bra-ket symbols and taken the periodic gauge. Besides, through the gauge symmetry (2.4) and (2.6), we have

$$p(\theta - 2\pi) = p(\theta) + 1. \quad (3.14)$$

By combining these two equations with $\theta = 0$ and π , we obtain

$$p(0) = 0, \quad p(\pi) = -\frac{1}{2}. \quad (3.15)$$

Actually, the analytic result is consistent with this relation as shown in Fig. 1 (center). Note that this result implies that the velocity $\langle \dot{x} \rangle = \langle p \rangle + \theta/2\pi$ always becomes zero at $\theta = 0$ and π .

⁷The Hilbert space in $-\infty < x < \infty$ and that of on S^1 are different. We have implicitly assumed that the system is in $-\infty < x < \infty$ when we derive (3.12).

Now, we consider the application of this result to the bootstrap analysis to determine the θ dependence at $\theta = 0$ and π . In Fig. 4, we have derived the curves $E(\langle \dot{x} \rangle)$, and we can read off E at $\langle \dot{x} \rangle = 0$. Since $\langle \dot{x} \rangle$ becomes zero at $\theta = 0$ and π , they may correspond to $E(\theta) = E(0)$ or $E(\pi)$. Here, we can determine whether these values are for $\theta = 0$ or π by using the result at the $a = 0$ case discussed in Appendix A.

Our model (2.1) at $a > 0$ can be regarded as a deformation of the $a = 0$ case, and we can easily see that the curves in Fig. 4 at $a > 0$ merge to the ones shown in Fig. 5 (right) as $a \rightarrow 0$. Besides, Fig. 5 tells us the values of E , p and θ at the point $\langle \dot{x} \rangle = 0$ for $a = 0$ as

$$(E, p, \theta) = (0, 0, 0), (1/8, -1/2, \pi), (1/2, 0, 0), (9/8, -1/2, \pi), (2, 0, 0), \dots \quad (3.16)$$

Since these points would continue to $E(\langle \dot{x} \rangle) = E(0)$ at $a > 0$, we can fix the values of θ for $E(0)$ from them. For example, for the first eigenstate at $a > 0$, there are two $E(\langle \dot{x} \rangle) = E(0)$ as we see in Fig. 4, and we can determine that the lower energy is for $\theta = 0$ and the higher one is for $\theta = \pi$ through (3.16). Thus, we obtain $E(\theta = 0) \simeq 0.31$ and $E(\pi) \simeq 0.33$ at $a = 1/2$ from Fig. 4.

Similarly, at the second eigenstate, the lower energy is for $\theta = \pi$ and the higher one is for $\theta = 0$. Generally, at the $(2n + 1)$ -th eigenstate, the lower one is for $\theta = 0$ and the higher one is for $\theta = \pi$, and it is opposite at the $2n$ -th eigenstate. They agree with the analytic result shown in Fig. 1 (left). In this way, we can determine $E(\theta = 0)$ and $E(\pi)$ ⁸. Once we obtain the energies at $\theta = 0$ and π , all other observables are determined through the correlations discussed above.

4 Discussions

In this article, we studied the θ dependence in the model (1.1), and found that the correct correlations among the observables can be derived. However, we failed to obtain the θ dependence of the observables except at $\theta = 0$ and π . Hence, the bootstrap method tells us, for example, that $E(\theta)$ for the n -th energy eigenstates is in the range shown in Fig. 3, and if one value of energy is given in this range, the values of the observables $\langle O_{mn} \rangle$ are determined. Thus, the bootstrap method provides us useful information but not as much as the analytic results derived in Sec. 2.

⁸Our derivation relies on the information of the $a = 0$ result. If we consider different systems with θ -terms, we may need to use alternative inputs. For example, see [20] for large- N gauge theories.

Our study reveals two interesting properties of the bootstrap method. The first one is that the method may work even if the system suffers sign problems, although it may fail in evaluating some quantities. We presume that, as far as the condition $\langle O^\dagger O \rangle \geq 0$ is satisfied for suitable observables O , the bootstrap method may work somehow⁹.

Another interesting property is that the bootstrap method may illuminate hidden natures of systems. Suppose that we did not know the existence of the θ -parameter in the system (1.1) and studied (2.1) with $\theta = 0$. Even in this case, the bootstrap method reproduces the results that take the θ dependence into account. Hence, by applying the bootstrap method to various systems, some unexpected new phenomena might be found.

One important challenge is overcoming the gauge fixing problem that prevents us from deriving the θ dependence of the observables. Another challenge is application of the bootstrap method to higher dimensional quantum field theories. If it is achieved, we can apply the bootstrap method to QCD and tackle the θ -term problem there.

Besides, there are several interesting large- N matrix models in zero and one dimensions, which suffer sign problems. (For example, the Lorentzian IKKT matrix model [22, 23] and the BFSS matrix theory [24, 25].) Thus, it must be valuable to test the bootstrap method in these models.

Acknowledgements The authors would like to thank Takehiro Azuma, Masaru Hongo and Asato Tsuchiya for valuable discussions and comments. A part of numerical computation in this work was carried out at the Yukawa Institute Computer Facility. The work of T. M. is supported in part by Grant-in-Aid for Scientific Research C (No. 20K03946) from JSPS.

A Analytic result at $a = 0$

In this appendix, we summarize the analytic results at $a = 0$ in (2.1), in which we can derive the solutions easily. The results at $a > 0$ can be regarded as deformations of $a = 0$ and the analysis at $a = 0$ may help us to understand the properties of the system at $a > 0$.

Under the gauge fixing $\psi(x + 2\pi) = \psi(x)$, we obtain the energy eigenfunction and its

⁹For real time evolution, although the condition $\langle O^\dagger O \rangle \geq 0$ is satisfied, (3.6) is not satisfied and (3.5) is replaced by the Heisenberg equation. Thus, the constraints are much weakened. Besides, the Heisenberg equations are differential equations and they may be incompatible with the inequality constraint $\mathcal{M} \succeq 0$. A similar issue occurs even in thermal equilibrium states. We will report this problem soon [21].

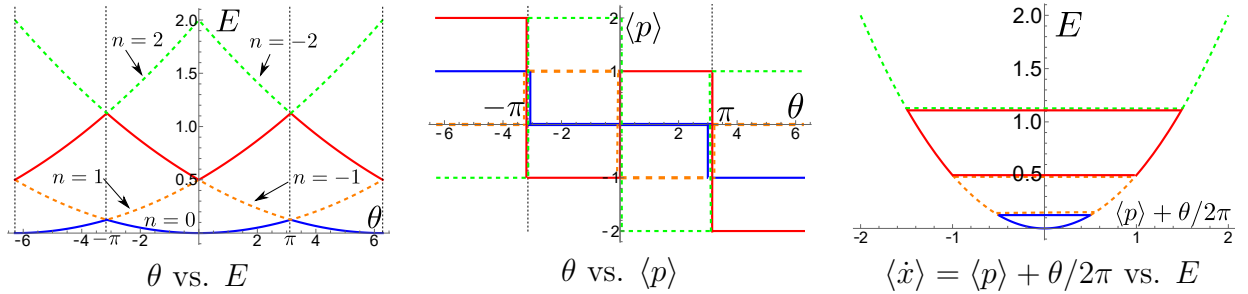


Figure 5: Analytic results at $a = 0$. We plot E and $\langle p \rangle$ for the first four eigenstates. The line styles correspond to those of Fig. 1. Although the graphs θ vs. E and θ vs. $\langle p \rangle$ are involved, the combined result $\langle \dot{x} \rangle$ vs. E becomes simpler.

energy eigenvalue,

$$\phi_n(x) := \frac{1}{\sqrt{2\pi}} e^{inx}, \quad E_n := \frac{1}{2} \left(n + \frac{\theta}{2\pi} \right)^2. \quad (\text{A.1})$$

Interestingly, the energy levels change depending on the values of θ . See Fig. 5 (left). At $\theta = 0$, $n = 0$ is the ground state, and the first excited state is $n = \pm 1$ and the degeneracy occurs. Higher excitations are given by $n = \pm 2, \pm 3, \dots$. For $0 < \theta < \pi$, the degeneracies at the excited states disappear. The ground state is $n = 0$, the first excited state is $n = -1$, and the second one is $n = 1$. At $\theta = \pi$, the ground state is $n = 0$ and $n = -1$, and they are degenerate. For $\pi < \theta < 2\pi$, the ground state is $n = -1$. In this way, although the Hamiltonian (2.1) at $a = 0$ is simple, the spectra show complicated θ dependence.

However, if we use the velocity $\langle \dot{x} \rangle = \langle p \rangle + \theta/2\pi$ (2.7), the complicated spectrums can be simplified. Here, the expectation value of the momentum $\langle p \rangle$ is easily computed, since ϕ_n in (A.1) is the eigenfunction of p with the eigenvalue n . Then, the θ dependence of $\langle p \rangle$ is plotted as in Fig. 5 (center). Note that, due to the degeneracies at $\theta = k\pi$, ($k \in \mathbf{Z}$), $\langle p \rangle$ becomes multiple values there. Although this θ dependence is involved, by combining (A.1) and (2.7), we obtain a simplified expression with respect to $\langle \dot{x} \rangle$,

$$E = \frac{1}{2} \left(\langle p \rangle + \frac{\theta}{2\pi} \right)^2 = \frac{1}{2} \langle \dot{x} \rangle^2. \quad (\text{A.2})$$

See Fig.5 (right). Again, due to the degeneracies at $\theta = k\pi$, multiple values appear at $E = k^2/8$.

If we compare the results at $a = 0$ (Fig. 5) and the ones at $a > 0$ (Fig. 1 and 2), we find that the latter can be regarded as a deformation of the former.

Bootstrap analysis Bootstrap analysis at $a = 0$ is special, since momentum is conserved and the energy eigenstate can be a momentum eigenstate. Thus, p can be treated as a c-number, and we obtain (A.2) directly. Besides, we can fix the gauge because $\langle e^{2\pi ip} \rangle = e^{2\pi i \langle p \rangle}$ and the periodicity of the states is controlled by the value of p . If we wish to take the gauge $\psi(x + 2\pi) = \psi(x)$, p is restricted to integers, and we reach the energy (A.1). Thus, without using a bootstrap, we obtain the solution merely through the symmetries.

On the other hand, it is possible to perform the standard bootstrap analysis, if we do not impose the condition that the states are eigenstates of momentum. Then, we obtain similar results to the ones in Sec. 3 at $a > 0$.

References

- [1] John R. Klauder. Coherent-state langevin equations for canonical quantum systems with applications to the quantized hall effect. *Phys. Rev. A*, 29:2036–2047, Apr 1984.
- [2] G. Parisi. ON COMPLEX PROBABILITIES. *Phys. Lett. B*, 131:393–395, 1983.
- [3] Gert Aarts, Erhard Seiler, and Ion-Olimpiu Stamatescu. Complex langevin method: When can it be trusted? *Phys. Rev. D*, 81:054508, Mar 2010.
- [4] Gert Aarts, Frank A. James, Erhard Seiler, and Ion-Olimpiu Stamatescu. Complex Langevin: Etiology and Diagnostics of its Main Problem. *Eur. Phys. J. C*, 71:1756, 2011.
- [5] Keitaro Nagata, Jun Nishimura, and Shinji Shimasaki. Gauge cooling for the singular-drift problem in the complex Langevin method - a test in Random Matrix Theory for finite density QCD. *JHEP*, 07:073, 2016.
- [6] Keitaro Nagata, Jun Nishimura, and Shinji Shimasaki. Argument for justification of the complex Langevin method and the condition for correct convergence. *Phys. Rev. D*, 94(11):114515, 2016.
- [7] Michael Levin and Cody P. Nave. Tensor renormalization group approach to 2D classical lattice models. *Phys. Rev. Lett.*, 99(12):120601, 2007.
- [8] Edward Witten. Analytic Continuation Of Chern-Simons Theory. *AMS/IP Stud. Adv. Math.*, 50:347–446, 2011.
- [9] Marco Cristoforetti, Francesco Di Renzo, and Luigi Scorzato. New approach to the sign problem in quantum field theories: High density qcd on a lefschetz thimble. *Phys. Rev. D*, 86:074506, Oct 2012.
- [10] Keitaro Nagata. Finite-density lattice QCD and sign problem: current status and open problems. 8 2021.

- [11] Peter D. Anderson and Martin Kruczenski. Loop Equations and bootstrap methods in the lattice. *Nucl. Phys. B*, 921:702–726, 2017.
- [12] Henry W. Lin. Bootstraps to strings: solving random matrix models with positvite. *JHEP*, 06:090, 2020.
- [13] Xizhi Han, Sean A. Hartnoll, and Jorrit Kruthoff. Bootstrapping Matrix Quantum Mechanics. *Phys. Rev. Lett.*, 125(4):041601, 2020.
- [14] Vladimir Kazakov and Zechuan Zheng. Analytic and Numerical Bootstrap for One-Matrix Model and "Unsolvable" Two-Matrix Model. 8 2021.
- [15] David Berenstein and George Hulsey. Bootstrapping Simple QM Systems. 8 2021.
- [16] Jyotirmoy Bhattacharya, Diptarka Das, Sayan Kumar Das, Ankit Kumar Jha, and Moulindu Kundu. Numerical Bootstrap in Quantum Mechanics. 8 2021.
- [17] David Tong. Lectures on Gauge Theory.
- [18] David Berenstein and George Hulsey. Bootstrapping More QM Systems. 9 2021.
- [19] Serguei Tchoumakov and Serge Florens. Bootstrapping Bloch bands. 9 2021.
- [20] Edward Witten. Theta dependence in the large N limit of four-dimensional gauge theories. *Phys. Rev. Lett.*, 81:2862–2865, 1998.
- [21] Yu Aikawa, Takeshi Morita, and Kota Yoshimura. On going work.
- [22] N. Ishibashi, H. Kawai, Y. Kitazawa, and A. Tsuchiya. A Large N reduced model as superstring. *Nucl. Phys. B*, 498:467–491, 1997.
- [23] Sang-Woo Kim, Jun Nishimura, and Asato Tsuchiya. Expanding (3+1)-dimensional universe from a Lorentzian matrix model for superstring theory in (9+1)-dimensions. *Phys. Rev. Lett.*, 108:011601, 2012.
- [24] Tom Banks, W. Fischler, S. H. Shenker, and Leonard Susskind. M theory as a matrix model: A Conjecture. *Phys. Rev.*, D55:5112–5128, 1997. [,435(1996)].
- [25] Konstantinos N. Anagnostopoulos, Masanori Hanada, Jun Nishimura, and Shingo Takeuchi. Monte Carlo studies of supersymmetric matrix quantum mechanics with sixteen supercharges at finite temperature. *Phys. Rev. Lett.*, 100:021601, 2008.